〈一般研究課題〉 単結晶マイクロピラー圧縮試験を用いた Al 合金積層造形体の 高強度および変形に対する微細構造寄与因子調査

助 成 研 究 者 名古屋大学 キム ダソム



# 単結晶マイクロピラー圧縮試験を用いた Al合金積層造形体の 高強度および変形に対する微細構造寄与因子調査

キム ダソム (名古屋大学)

Microstructural contributors to high strength and deformation of additive
manufactured Al alloy using via single-crystal micropillar compression test approach

Dasom Kim
(Nagoya University)

## Abstract:

This study investigated microstructural contributors of high strength and unique deformation in Al-2.5 (mass%)Fe alloy manufactured via laser beam powder bed fusion (L-PBF) under rapid cooling rate. The as-built Al-Fe alloy has an inhomogeneous melt-pool structure, where the melt-pool boundary (MPB), formed at relatively lower cooling rates, surround the melt-pool interior (MPI). The local mechanical properties of MPIa and MPB were evaluated using single-crystal micropillar compression tests. The MPI exhibited higher stress (252 MPa) compared to the MPB. This is attributed to the microstructural origins of MPI where the nano-sized metastable Al<sub>6</sub>Fe, and supersaturated Fe (0.64 at%) in Al matrix, exceeding its soluability limit (<0.05 at%). Notably, the MPI has negative strain rate sensitivity (SRS) of flow stress. The MPI maintained a multi-slip system regardless of initial strain rate, suggesting that the negative SRS is not associated with a slip system transition. Transmission electron microscopy analysis of the compression tested micropillars revealed that dislocations interacted with the nano-sized Al<sub>6</sub>Fe that was dynamically precipitated from the supersaturated Fe under the deformation. This dynamic precipitation hardening is identified as the primary cause of negative SRS of MPI.

## 1. Introduction

Al-Fe binary system alloys have potential to be used for heat exchanger, cylinder head, landing gear, engine cover in aerospace, automobile, electric, energy industries due to advantages such as high-specific strength [1], and thermal conductivity[2]. The key factor contributing to these superior properties is the Al-Fe intermetallic compounds ( $\theta$ -Al<sub>13</sub>Fe<sub>4</sub> phase), which is a thermodynamically stable phase in the Al-Fe binary system [3]. It was reported that the  $\theta$ -Al<sub>13</sub>Fe<sub>4</sub> phase contributed to enhanced strength and thermal stability by acting as a reinforcing phase within the Al matrix, whereas the  $\theta$ -Al <sub>13</sub>Fe<sub>4</sub> significantly deteriorated the ductility due to its intrinsic brittleness at ambient temperature and the stress concentration due to its plate- or needle-shaped morphology [4, 5]. This excessive formation of brittle  $\theta$ -Al <sub>13</sub>Fe<sub>4</sub> limits the practical applicability of Al-Fe alloys, especially in components requiring complex geometries and high mechanical reliability, such as heat sinks in electronic devices or lightweight structural materials in transportation sectors. To overcome these limitations, it is necessary to develop advanced processing techniques that enable precise control of the formation, morphology, and spatial distribution of Al-Fe intermetallic phases, thereby optimizing the mechanical properties of the alloy without compromising its manufacturability.

Additive manufacturing (AM), also known as 3D printing, is a process that creates three-dimensional solid objects layer-by-layer that enables to manufacture complex-shaped 3D parts. Laser beam powder bed fusion (PBF-LB) process is one of representative metal AM [6] [7] and characterized via super rapid cooling rate (10<sup>5</sup> to 10<sup>7</sup> °C/s [8]) compared to that of conventional manufacturing processed such as casting (~0.1<sup>-1</sup>°C/s). Al-Fe alloys manufactured PBF-LB process have non-equilibrium solidification microstructure with unique microstructural features [9, 10]: (1) distribution of nano-sized Al<sub>6</sub>Fe metastable phase (orthorhombic, oC24) within Al matrix where (2) the supersaturation of Fe content exceeding the low solubility limits of Fe in Al (0.05 at%), resulting in the enhanced mechanical properties and their high thermal stability compared to the cast Al-Fe alloy [11, 12].

The PBF-LB manufactured Al-Fe alloys have inhomogeneous melt-pool structure that the melt-pools were stacked layer by layer. Unique microstructural features are remarkable in the melt-pool interior (MPI) with much higher cooling rate than melt-pool boundary (MPB) where the solidification is started. The temperature gradient ( $G_T$ ) and growth rate of solid ( $R_S$ ) are changed in a melt-pool, the heat flow in the melt-pool causes directional solidification from the solid/liquid interface (corresponding to the melt-pool boundary: MPB) with minimum cooling rate ( $G_T \times R_S$ ) due to lower  $R_S$  toward the melt-pool interior (MPI) [8, 13, 14]. Since the PBF-LB processed Al-Fe alloys have inhomogeneous melt-pool structure [11], [15] [16], it is necessary to investigate the different mechanical response of MPI and MPB, respectively. However, it is still unclear that the microstructural origins of high strength and deformation mechanism of PBF-LB Al-Fe alloys due to the experimental limit.

The single-crystal micropillar compression test is a promising micromechanical testing technique

combined to the crystallographic orientation analysis to investigate the local mechanical properties and deformation mechanism in submicron scale single crystal [17]. Single-crystal micropillar compression has also been used to explore strain rate sensitivity (SRS) [18] that is one of parameter to assess hot workability [19]. Fcc metals including Al alloys exhibit classic positive SRS, whereas we recently discovered hitherto unforeseen mechanical behavior (i.e. negative strain rate sensitivity (SRS) of flow stress during the early stages of deformation of the MPI of Al-2.5 (mass%) Fe alloy manufactured via PBF-LB process, using single-crystal micropillar compression test. To elucidate the origin of this anomalous negative SRS, it is necessary to investigate the dynamic precipitation behaviour at different strain rates.

This study aimed to reveal the microstructural contributors of high strength and the deformation mechanism in L-PBF Al-2.5Fe alloy through single-crystal micropillar compression tests. Specifically, we focused on identifying the dynamic precipitation behaviour associated with negative SRS of MPI. As a first step, we analysed the mechanical inhomogeneity in the melt-pool structure of the Al-Fe alloy manufactured via L-PBF process, conducting micropillar compression tests in different local regions (MPI and MPB).

## 2. Experimental procedure

L-PBF process was performed using a gas atomized Al-2.5Fe (wt%) alloy powder with a mean particle size of about 20 µm and a 3D system ProX 200 equipped with a Yb-fiber laser (laser power: 204 W, scanning speed: 0.6 m/s). To observe the melt-pool structure of L-PBF processed Al-2.5Fe alloy, the cross-section was observed via an optical microscope after chemical etching with a 3% hydrofluoric acid aqueous solution. The crystallographic orientations of Al grains were determined via a scanning electron microscope (SEM, JEOL JSM- 7001FA, Japan) and electron backscattered diffraction (EBSD) analysis on the electropolished cross-section. The microstructures of MPI and MPB were characterized via transmission electron microscope (TEM, JEOL JEM-2100 Plus, Japan) operated at 200 kV and the element composition of solute Fe was measured using by energy dispersive X-ray spectroscopy (EDS) point analysis. Multiple cylindrical micropillars with a diameter of 2 µm on the MPB and MPI within a single crystal grain were prepared using the focused ion beam (FIB, JEM-9320, Japan) with a JEOL JSM-9320 operated at 30 kV. Uniaxial compression tests on the micropillars were conducted using a nanoindenter equipped with a flat-tip indenter with a diameter of 20 µm (DUH- 211 S, SHIMADZU, Japan). Compression tests were performed at different initial strain rates (\(\bar{\epsilon}\)) in the range of 10-6 to 10-1 s-1 controlled by changing the loading rate ( $\Delta F$ ) [31]. The strain rate sensitivity (m) was obtained using the equation using initial stress ( $\sigma_i$ ) and initial strain rate ( $\dot{\varepsilon}$ ).

 $m = \partial ln \sigma_i / \partial ln \varepsilon_i$ 

Slowly cooled Al-2.5Fe alloy was prepared via furnace cooling system where the gas atomized Al-2.5 Fe (mass%) alloy powder was melted at 940 °C under low cooling rate (0.3°C/s) as a reference sample to compare the strain rate sensitivity with L-PBF Al-2.5Fe alloy. The cross

section of compression-tested micropillars were analyzed via TEM.

#### 3. Results

The LPBF processed Al-2.5Fe alloy exhibits the microstructure that melt pools with a depth of approximately 100 µm were stacked with the building direction (Z), shown in Fig. 1(a). The melt-pool boundary (MPB) with a thickness of 2~3 μm (Fig. 1(b)) surrounds the melt-pool interior (MPI). Fig. 1(c) and (d) show the STEM dark-field images obtained on the MPI and MPB, respectively. A number of nanosize particles (Al6Fe metastable phase) are homogenously distributed within Al grains of the MPI, while the few Al<sub>6</sub>Fe phase was found in MPB. The solute Fe concentrations in the α-Al grain of MPI and MPB measured by EDS point analysis were 1.4 mass% and 0.6 mass%, respectively. The solute contents of Fe on both MPI and MPB are over the solubility limit of Fe in Al (approximately 0.05 wt%), which indicates solute Fe is supersaturated in Al grains.

Fig. 2 presents the summarized information obtained about the preparation of single crystal

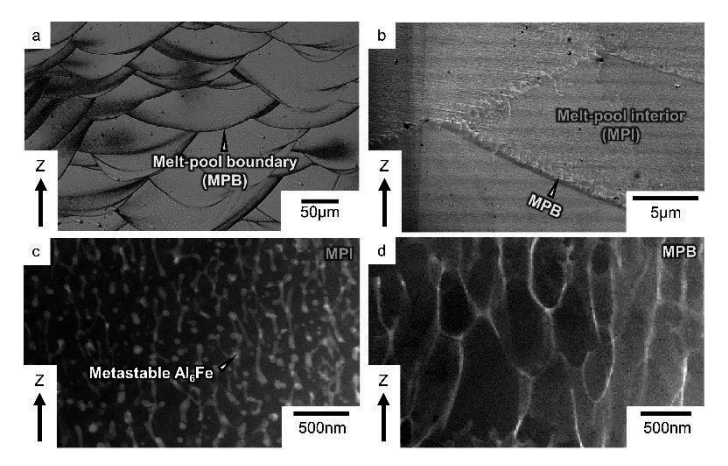


Fig. 1. Microstructures showing the cross section of L-PBF processed Al-2.5Fe alloy: (a) optical image and (b) SEM image showing melt-pool structure, Scanning-TEM dark-field images of (c) MPI and (d) MPB.

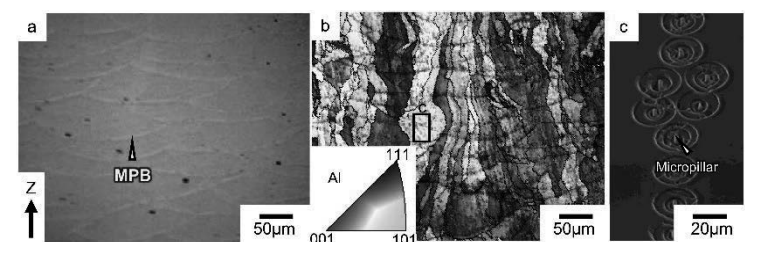


Fig. 2. (a) SEM image and (b) EBSD IPF + IQ maps of L-PBF processed Al-2. 5Fe alloy. SEM image showing (c) a single grain of L-PBF processed Al-2.5Fe alloy where multiple micropillars.

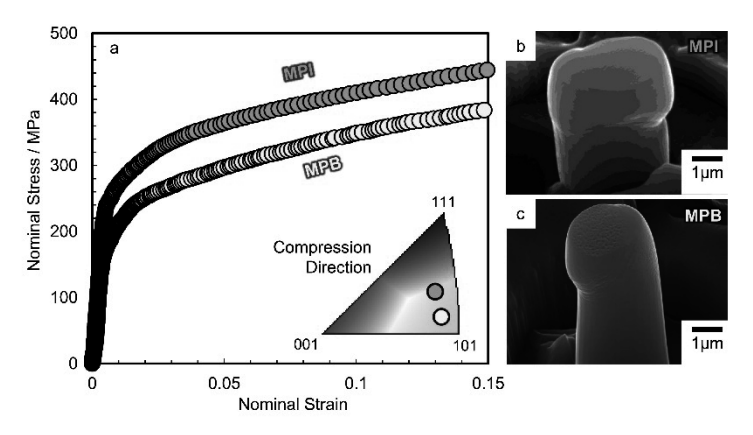


Fig. 3. (a) Nominal stress-strain curves of single-crystal micropillars of MPI and MPB in the melt-pool structure. (b, c) SEM images showing the compression-tested micropillars prepared from (b) MPI and (c) MPB.

micropillars on the MPI and MPB of L-PBF processed Al-2.5Fe alloy, respectively. The MPB with brighter contrast was clearly observed on the electropolished cross-section, shown in Fig. 2(a). EBSD IPF map obtained on such cross-section shows the crystal grains of the α-Al grains and combined with image quality (IQ) map to clearly find the MPB with dark contrast due to the coarsened Al<sub>6</sub>Fe particles, shown in Fig. 2(b). The L-PBF processed Al- 2.5Fe alloy exhibited columnar Al grains elongated along the building direction (Z) In a single crystal indicated as a

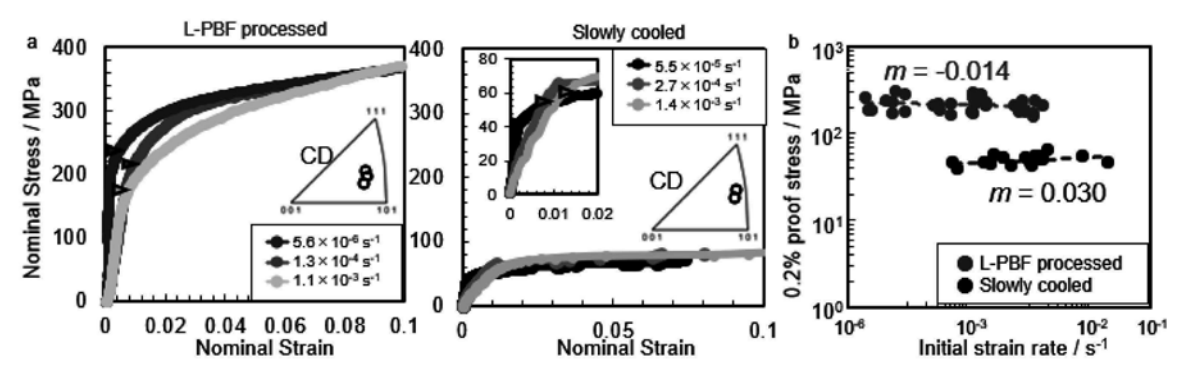


Fig. 4. (a) Nominal stress-strain curves of single-crystal micropillars of MPI in L-PBF processed and slowly cooled Al-2.5Fe alloy, (b) 0.2% proof stress as a function of initial strain rate.

rectangle box, multiple micropillars with a diameter of 2 μm (Fig. 2(c)) were prepared using the FIB system.

Fig. 3 shows the single-crystal micropillar compression test results of MPI and MPB. An attached unit triangle of the inverse pole figure indicates the compression direction of each single crystal of the L-PBF processed Al-2.5Fe alloy. The nominal stress-strain curves of the single-crystal micropillars prepared on the MPI and MPB within a single grain are

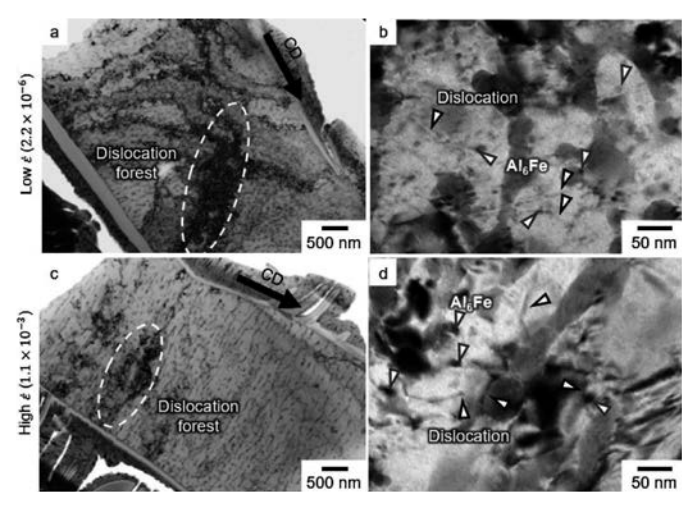


Fig. 5. TEM analysis results of compression tested micropillars of asbuilt Al-Fe alloy: (a-d) bright field TEM images of compression tested micropillars of as-built Al-Fe alloy at (a,b) low and (c,d) high initial strain-rate.

shown in Fig. 3(a). The compression direction is indicated on the unit triangle of the IPF. The 0.2% proof stress of MPI (250 MPa) is higher than that of MPB (170 MPa) due to different microstructural features such as distribution of refined Al<sub>6</sub>Fe phase and solute Fe content in Al grains. The SEM images of compressed single-crystal micropillars of MPI (Fig. 3(b)) and MPB (Fig. 3(c)) shows the presence of macroscopic slip traces on their cylindrical surfaces and, hence, the activation of multi-slip systems.

Fig. 4(a) presents the nominal stress-strain curves of MPI of L-PBF processed and Slowly cooled Al-2.5Fe alloys obtained at various  $\dot{\varepsilon}$  in a range of  $10^{-6}$  to  $10^{-1}$ s<sup>-1</sup>. The CDs are indicated on the unit triangle of IPFs. The 0.2% proof stress ( $\sigma_{0.2}$ ) were indicated on the graphs via triangle on the stress-strain curves. Whole  $\sigma_{0.2}$  values obtained at various  $\dot{\varepsilon}$  were plotted as a function of  $\dot{\varepsilon}$ , shown in Fig. 4(b). The slowly cooled Al-Fe alloys have positive m values of 0.030, whereas the L-PBF processed Al-2.5Fe alloy showed negative m value of -0.014.

Fig. 5 shows the TEM images of compression tested micropillars at (a,b) low and (c,d) high  $\dot{\varepsilon}$ . Larger amount of dislocations accumulated in the compression tested micropillars at lower  $\dot{\varepsilon}$  accumulated (Fig. 5 (a,c)). In the dislocation forest, nano-sized Al<sub>6</sub>Fe particles that have dark contrasts

interacted with the dislocations (Fig. 5(b,d)). Fine  $Al_6Fe$  phase would be precipitated from saturated Fe in Al matrix due to the lattice distortion during the compression test. That is, the nucleation of very fine  $Al_6Fe$  phases contributed to the strengthening by the interaction with dislocations.

#### References

- [1] T. Kimura, T. Nakamoto, T. Ozaki, T. Miki, Microstructures and mechanical properties of aluminum-transition metal binary alloys (Al-Fe, Al-Mn, and Al-Cr) processed by laser powder bed fusion, Journal of Alloys and Compounds, 872 (2021) 159680.
- [2] Y. Liu, Y. Liu, S. Akhtar, P. Wang, Z. He, X. Jiao, S. Ge, G. Yuan, Y. Zhang, X. Li, Thermal conductivity of binary Al alloys with different alloying elements, Journal of Alloys and Compounds, 1010 (2025) 177257.
- [3] T. Dorin, N. Stanford, N. Birbilis, R. Gupta, Influence of cooling rate on the microstructure and corrosion behavior of Al-Fe alloys, Corrosion Science, 100 (2015) 396-403.
- [4] Y. Xue, R. Shen, S. Ni, M. Song, D. Xiao, Fabrication, microstructure and mechanical properties of Al-Fe intermetallic particle reinforced Al-based composites, Journal of Alloys and Compounds, 618 (2015) 537-544.
- [5] T. Tsukahara, N. Takata, S. Kobayash, M. Takeyama, Mechanical properties of Fe2Al5 and FeAl3 intermetallic phases at ambient temperature, TETSU TO HAGANE-JOURNAL OF THE IRON AND STEEL INSTITUTE OF JAPAN, 102 (2016) 29-35.
- [6] S.L. Sing, W.Y. Yeong, Laser powder bed fusion for metal additive manufacturing: perspectives on recent developments, Virtual and Physical Prototyping, 15 (2020) 359-370.
- [7] W. Abd-Elaziem, S. Elkatatny, A.-E. Abd-Elaziem, M. Khedr, M.A. Abd El-baky, M.A. Hassan, M. Abu-Okail, M. Mohammed, A. Järvenpää, T. Allam, On the current research progress of metallic materials fabricated by laser powder bed fusion process: a review, Journal of Materials Research and Technology, 20 (2022) 681-707.
- [8] N. Takata, M. Liu, H. Li, A. Suzuki, M. Kobashi, Fast scanning calorimetry study of Al alloy powder for understanding microstructural development in laser powder bed fusion, Materials & Design, 219 (2022) 110830.
- [9] X. Qi, N. Takata, A. Suzuki, M. Kobashi, M. Kato, Managing both high strength and thermal conductivity of a laser powder bed fused Al- 2.5 Fe binary alloy: Effect of annealing on microstructure, Materials Science and Engineering: A, 805 (2021) 140591.
- [10] X. Qi, N. Takata, A. Suzuki, M. Kobashi, M. Kato, Change in microstructural characteristics of laser powder bed fused Al-Fe binary alloy at elevated temperature, Journal of Materials Science & Technology, 97 (2022) 38-53.
- [11] W. Wang, N. Takata, A. Suzuki, M. Kobashi, M. Kato, High-temperature strength sustained by nano-sized eutectic structure of Al-Fe alloy manufactured by laser powder bed fusion, Materials Science and Engineering: A, 838 (2022) 142782.

- [12] A. Medvedev, M. Murashkin, N. Enikeev, E. Medvedev, X. Sauvage, Influence of morphology of intermetallic particles on the microstructure and properties evolution in severely deformed Al-Fe alloys, Metals, 11 (2021) 815.
- [13] M.-S. Pham, B. Dovgyy, P.A. Hooper, C.M. Gourlay, A. Piglione, The role of side-branching in microstructure development in laser powder-bed fusion, Nature communications, 11 (2020) 749.
- [14] B. Fotovvati, S.F. Wayne, G. Lewis, E. Asadi, A Review on Melt Pool Characteristics in Laser Welding of Metals, Advances in Materials Science and Engineering, 2018 (2018) 4920718.
- [15] X. Qi, N. Takata, A. Suzuki, M. Kobashi, M. Kato, Laser powder bed fusion of a near-eutectic Al-Fe binary alloy: Processing and microstructure, Additive Manufacturing, 35 (2020) 101308.
- [16] X. Qi, N. Takata, A. Suzuki, M. Kobashi, M. Kato, Controllable tensile performance of additively manufactured Al-Fe alloy, Materials Science and Engineering: A, 855 (2022) 143893.
- [17] J. Schwiedrzik, R. Raghavan, A. Bürki, V. LeNader, U. Wolfram, J. Michler, P. Zysset, In situ micropillar compression reveals superior strength and ductility but an absence of damage in lamellar bone, Nature materials, 13 (2014) 740-747.
- [18] Z. Zhang, T.-S. Jun, T.B. Britton, F.P. Dunne, Intrinsic anisotropy of strain rate sensitivity in single crystal alpha titanium, Acta Materialia, 118 (2016) 317-330.
- [19] M. Zhao, L. Huang, C. Li, J. Li, P. Li, Evaluation of the deformation behaviors and hot workability of a high-strength low-alloy steel, Materials Science and Engineering: A, 810 (2021) 141031.